Studies of electron–phonon and phonon–phonon interactions in InN using ultrafast Raman spectroscopy

2009 J. Phys.: Condens. Matter 21 174202

(http://iopscience.iop.org/0953-8984/21/17/174202)

J. Phys.: Condens. Matter **21** (2009) 174202 (7pp) doi:10.1088/0953-8984/21/17/174202

Studies of electron–phonon and phonon–phonon interactions in InN using ultrafast Raman spectroscopy

K T Tsen[1,3] **and D K Ferry**[2]

[1] Department of Physics, Arizona State University, Tempe, AZ 85287, USA
[2] Department of Electrical and Computer Engineering, Arizona State University, Tempe, AZ 85287, USA

E-mail: tsen@asu.edu

Received 3 October 2008, in final form 6 January 2009
Published 1 April 2009
Online at stacks.iop.org/JPhysCM/21/174202

Abstract
Subpicosecond time-resolved Raman spectroscopy has been employed to investigate electron–phonon interactions and phonon dynamics in InN. The electron–longitudinal optical phonon scattering rate and the decay dynamics of longitudinal optical phonons in InN have been directly measured. Our results indicate that hot-phonon effects can play an important role in the electron relaxation and transport in InN. The carrier dependence of the lifetime of the longitudinal optical phonons has also been measured. The results suggest that more theoretical work is needed to account for the dependence of the lifetime of longitudinal optical phonons on the photoexcited carrier density.

1. Introduction

The recent surge of activity in nitride-based semiconductors [1] has arisen from the need for electronic devices capable of operation at high power levels, high temperatures and caustic environments, and separately, from a need for optical materials, especially emitters, which are active in the blue and ultraviolet wavelengths. Electronics based upon the existing semiconductor device technologies of Si and GaAs cannot tolerate greatly elevated temperatures or chemically hostile environments. The wide bandgap semiconductors with their excellent thermal conductivities, large breakdown fields, and resistance to chemical corrosion will be the materials of choice for these applications. Among the wide bandgap semiconductors, the III–V nitrides have long been viewed as a very promising semiconductor system for device applications in the blue and ultraviolet wavelengths. The wurtzite polytypes of GaN, AlN, and InN form a continuous alloy system whose direct bandgaps range from 0.8 eV for InN, to 3.4 eV for GaN, to 6.2 eV for AlN. Thus III–V nitrides could potentially be fabricated into optical devices which are active at wavelengths ranging from the red all the way into the ultraviolet.

Recent progress in the manufacturing of very high quality, single-crystal InN thin films has opened up a new challenging research avenue in the III-nitride semiconductors [2]. It has also been predicted that InN has the lowest electron effective mass among all the III-nitride semiconductors [3]. As a result, very high electron mobility and very large saturation velocity are expected. It was found by ensemble Monte Carlo (EMC) simulations that InN possesses extremely high transient electron drift velocity [4–6]. Although much progress has been made in the device-oriented applications with wide bandgap semiconductors, very little information concerning their dynamical properties has yet been obtained. Knowledge of both carrier and phonon dynamical properties is indispensable for device engineers to design better and faster devices. For example, carrier energy loss rate is primarily determined by electron–phonon scattering rates [7]; electron relaxation may be greatly influenced by the hot-phonon effects [8] which in turn are governed by the population relaxation time of optical phonons. In this paper, electron–phonon interactions and non-equilibrium phonon dynamics in InN are studied by using ultrafast Raman spectroscopy.

2. Sample

The sample studied in this work was a thick InN film grown on HVPE GaN template by conventional MBE technique [9]. RF-remote plasma nitrogen was supplied by an EPI Unibulb

[3] Author to whom any correspondence should be addressed.

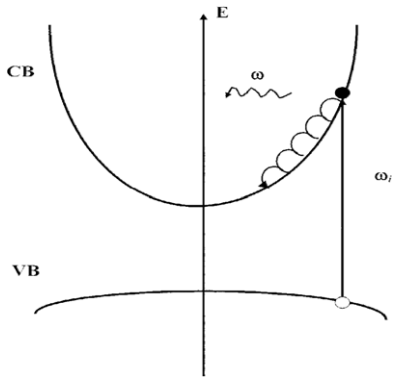

Figure 1. Band structure diagram showing how the non-equilibrium phonons are generated by a laser with photon energy above the bandgap of a direct semiconductor. CB: conduction band; VB: valence band; ω_i indicates the incident photon; ω corresponds to the emitted phonons.

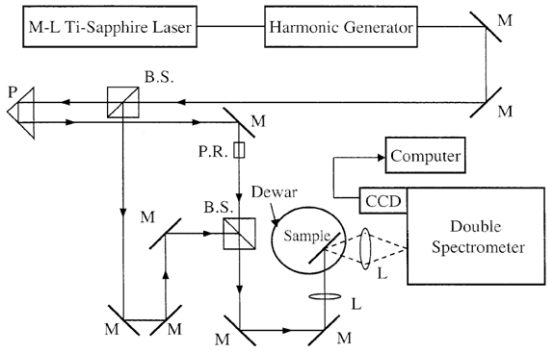

Figure 2. Experimental setup for subpicosecond time-resolved Raman scattering experiments. M: mirror; P: prism; B.S.: beam splitter; P.R.: polarization rotator; L: lens; CCD: charge-coupled device.

source operating at 260 W with 0.7 sccm nitrogen flow. Prior to InN growth, the substrate was directly heated to 525 °C, measured by thermocouple, then InN growth was started. The InN growth rate was about 0.7 μm h^{-1} with final film thickness around 7.5 μm. The HVPE GaN template has been compensated with Zn introduced during growth to suppress unintentional n-type conductivity. Its thickness was around 16 μm with 300 K resistivity up to 10^9 Ω cm and dislocation density around 5×10^8 cm^{-2}. The InN film was n-type and had an electron density of $\cong 5 \times 10^{17}$ cm^{-3}.

3. Experimental approach and experimental setup

3.1. Experimental approach for the studies of electron–phonon interactions and phonon dynamics in semiconductors

Subpicosecond time-resolved Raman spectroscopy can be used to directly study non-equilibrium electron–phonon and phonon–phonon interactions in III–V compound semiconductors. As shown in figure 1, electron–hole pairs are photoexcited by a subpicosecond excitation laser pulse either across the bandgap of the III–V semiconductors such as InN either directly (in the case of above-bandgap excitation) or through non-linear processes (in the case of below-bandgap excitations). These energetic electron–hole pairs will relax to the bottom of the conduction band (for electrons) and to the top of the valence band (for holes) by emitting non-equilibrium phonons through electron–phonon interactions [7]. By monitoring the occupation number of these emitted non-equilibrium phonons with a suitably time-delayed subpicosecond laser pulse, information such as the strength of electron–phonon interactions and phonon–phonon interactions can be readily obtained.

3.2. Experimental setup

The experimental setup for time-resolved subpicosecond Raman spectroscopy is shown in figure 2 [10–13]. The output of the second harmonic generation of a mode-locked Ti–sapphire laser was used as both the excitation and probing sources in our pump/probe experiments. The laser, which had a repetition rate of 80 MHz and a pulse width of about 100 femtoseconds, was chosen to operate at a wavelength of 442 nm. In the pump/probe configuration, the ultrashort pulse train was split into two beams of equal intensity but different polarization. One of the beams was used for the excitation of non-equilibrium phonons; the other, after being appropriately time-delayed, was used for probing the non-equilibrium phonons through Raman spectroscopy. An appropriate analyzer was placed in front of the entrance of the spectrometer so that scattered light from the pump pulse was minimized while that from the probe pulse was allowed to be detected. The Raman signal was collected and analyzed by a standard computer-controlled Raman system which included a Spex 1403 double monochromator (with its middle slits wide open), a CCD detector and its associated electronics. All the experimental data were taken at $T = 10$ K. The photoexcited electron–hole pair density was estimated from the average laser power, the focused spot size on the sample surface and the absorption depth at the excitation laser wavelength. The zero delay at the sample was determined to within ± 0.01 ps by the observance of the interference effect which occurred when the pump and probe pulses were spatially and temporally overlapped.

4. Experimental results

4.1. Subpicosecond time-resolved Raman studies of electron–longitudinal optical phonon interactions in InN [14]

The energy difference between the A_1(LO) and E_1(LO) phonons is much smaller than the spectral width (FWHM $\cong$ 120 cm^{-1}) of the cw mode-locked Ti–sapphire laser used in our time-resolved Raman scattering experiments. In order to measure their lifetimes without confusion, we need to separate their contributions by using appropriate Raman scattering configurations. This separation can be achieved by using the second harmonic of a cw mode-locked YAlG laser as the excitation source which had wavelength at $\lambda = 532$ nm, a pulse width of about 70 ps and a spectral width of FWHM $\cong$ 1 cm^{-1}. Figures 3(a) and (b) show typical Stokes and

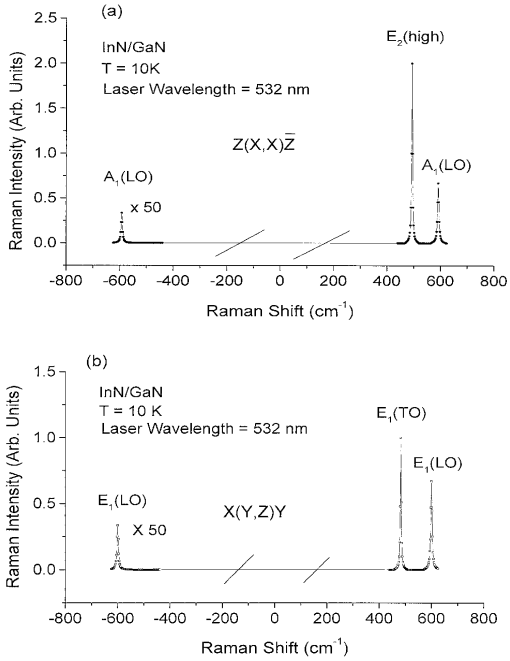

Figure 3. Typical Stokes and anti-Stokes Raman scattering spectra of the InN thick film grown on GaN taken for two scattering configurations: (a) $Z(X, X)\bar{Z}$, (b) $X(Y, Z)Y$, as indicated, at $T = 10$ K and by the second harmonic of a cw mode-locked YAlG laser. The excitation laser has wavelength at $\lambda = 532$ nm, a pulse width of about 70 ps and a spectral width of FWHM $\cong 1$ cm^{-1}.

anti-Stokes Raman scattering spectra of the sample taken for two scattering configurations: $X(Y, Z)Y$, $Z(X, X)\bar{Z}$, as indicated, at $T = 10$ K and by the second harmonic of a cw mode-locked YAlG laser. Here, $X = (100)$, $Y = (010)$ and Z is the direction parallel to the [0001] axis. The Raman modes are identified with the help of the Raman selection rules for wurtzite semiconductors. The observation of LO phonon modes on the anti-Stokes side of Raman spectra at such a low temperature as $T = 10$ K, indicates that energetic electrons relax toward the bottom of conduction band primarily by emitting LO phonons [7]. The most important aspect of these spectra is that under the $X(Y, Z)Y$ scattering configuration, only the E_1(LO) phonon mode contributes to the anti-Stokes signal; whereas under the $Z(X, X)\bar{Z}$ geometry, only the A_1(LO) phonon mode does. This intriguing aspect has been used in our time-resolved Raman experiments to measure the strength of electron–phonon interactions for the E_1(LO), A_1(LO) phonons, respectively, with the cw mode-locked Ti–sapphire laser; in other words, we use $Z(X, X)\bar{Z}$ scattering configuration for the measurement of the lifetime of A_1(LO) phonons and $X(Y, Z)Y$ for the determination of the lifetime of E_1(LO) phonons in our time-resolved Raman experiments.

A typical integrated anti-Stokes Raman intensity for the A_1(LO) phonon mode as a function of time delay and with a photoexcited electron–hole pair density $n \cong 1 \times 10^{16}$ cm^{-3}, is shown in figure 4. The very rapid rise of the signal from around $\Delta t = 0$ is a manifestation of an extremely large electron–LO phonon interaction in InN. It reaches a maximum at about 600 fs, indicative of the fact that at such a delayed

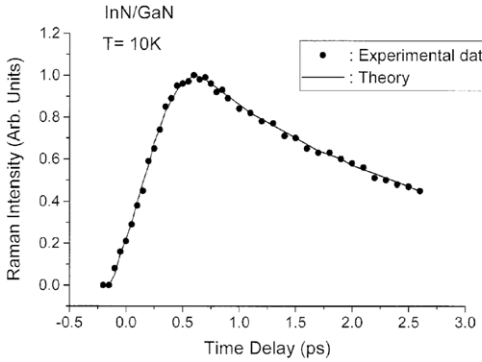

Figure 4. A typical integrated anti-Stokes Raman intensity for the A_1(LO) phonon mode in InN thick film grown on GaN as a function of time delay and with a photoexcited electron–hole pair density $n \cong 1 \times 10^{16}$ cm^{-3}. The solid circles are experimental data and the curve is the fit with equation (1).

time electrons are no longer emitting LO phonons that are detectable by our Raman spectroscopy. After about 600 fs, the anti-Stokes Raman intensity decreases with a decay constant of $\tau_{ph} = (2.2 \pm 0.2)$ ps.

To get better insight on electron–LO phonon interactions, we have used an electron cascade model to fit the experimental data in figure 4. The use of an electron cascade model under our experimental conditions is appropriate because: (1) the electron–hole pair density excited is low ($n \cong 10^{16}$ cm^{-3}); consequently, the effects of electron–electron interaction are minimal; and (2) the electrons do not have sufficient excess energy to scatter to other satellite valleys in InN [15]; as a result they will relax through the intravalley scattering processes in the Γ-valley.

In this model, the non-equilibrium LO phonon occupation number $n_{ph}(t)$ is given by the following rate equation:

$$\frac{dn_{ph}(t)}{dt} = G(t) + \frac{n_{ph}(t)}{\tau_{ph}}; \tag{1}$$

where $G(t)$ is the LO phonon generation rate by the excitation laser pulse and τ_{ph} is the LO phonon lifetime corresponding to the decay of the non-equilibrium phonons. For our current experimental conditions, the LO phonon generation rate is given by the approximation (the actual generation rate is a detailed function of the energy-dependent distribution function of the electrons at each step of the phonon cascade)

$$G(t) = \frac{f(t)}{\tau_{el-ph}}; \tag{2}$$

where $f(t) = 1$ for $0 \leqslant t \leqslant m\tau_{el-ph}$; and $f(t) = 0$ for $t \leqslant 0$ or $t \geqslant m\tau_{el-ph}$; τ_{el-ph} is the average electron–LO phonon scattering rate; m is an integer determined by the excitation photon energy, LO phonon energy, bandgap and bandstructure of wurtzite InN.

For wurtzite InN, we use the energy-dependent electron effective mass $m_e^*(E)$ [15] derived by a modified local-density approximation, which has been demonstrated to predict the correct bandgap energy of InN [16–20] and is also consistent with other measured electron effective masses around the Γ

valley. In addition, we take $m_h^* = 1.63m_e$ [21]; $\hbar\omega_i = 2.81$ eV; $E_g = 0.8$ eV; the index of refraction $n = 2.9$[4]; $\hbar\omega_{LO} = 0.075$ eV (corresponding to the A_1(LO) phonon energy). However, due to conservation of both energy and momentum for the electron–LO phonon interaction process there exists a range of LO phonon wavevectors that electrons can emit. For an electron with wavevector $\vec{k}_e$ and excess energy ΔE_e, the minimum and maximum LO phonon wavevectors it can interact with are given by [11]

$$k_{min} = \frac{\sqrt{2m_e^*}}{\hbar}(\sqrt{\Delta E_e} - \sqrt{\Delta E_e - \hbar\omega_{LO}}) \quad (3)$$

and

$$k_{max} = \frac{\sqrt{2m_e^*}}{\hbar}(\sqrt{\Delta E_e} + \sqrt{\Delta E_e - \hbar\omega_{LO}}). \quad (4)$$

Because of the nature of energy wavevector relationship of the electron, the lower the electron energy, the larger the k_{min} and the smaller the k_{max}. Therefore at some electron energy, the k_{min} of LO phonon will be larger than the wavevector ($q = 8.24 \times 10^5$ cm^{-1}) probed by our Raman scattering experiments. When that happens during the relaxation process, the energetic electrons can no longer emit LO phonons with wavevector detectable in our Raman scattering experiments. By taking this into consideration, we have found that although in principle the energetic electrons are capable of emitting 25 LO phonons during their thermalization to the bottom of the conduction band, only 15 of them can be detected in our Raman experiments; in other words, $m = 15$ under our current experimental conditions.

Therefore, there are two adjustable fitting parameters in this electron cascade model: phonon lifetime (τ_{ph}) and the average electron–phonon scattering time (τ_{el-ph}). However, because the LO phonon lifetime τ_{ph} can be independently measured from the decaying part of the Raman signal (as shown in figure 4), the average electron–LO phonon scattering time τ_{el-ph} is used as the only adjustable parameter in the fitting process.

We have found that $\tau_{el-ph} = (40 \pm 4)$ fs best fit the experimental data in figure 4, which gives rise to an electron–LO phonon scattering rate of $\Gamma_{el-ph} = 1/\tau_{el-ph} = (2.5 \pm 0.3) \times 10^{13}$ s^{-1}.

Similar experiments for the E_1(LO) phonon mode were also carried out (which are not shown). Our experimental results in this case show that the average electron–LO phonon scattering rate for E_1(LO) phonon mode is given by $\Gamma_{el-ph} = (2.6 \pm 0.3) \times 10^{13}$ s^{-1}, which is very close to the value found for A_1(LO) phonon.

Therefore, the average total electron–LO phonon scattering rate in InN is given by $\Gamma_{total} = (5.1 \pm 1.0) \times 10^{13}$ s^{-1}. Since the average electron–LO phonon scattering rate in GaAs (see footnote 4) is about 5×10^{12} s^{-1}, the observed average total electron–LO phonon scattering rate in wurtzite InN is almost one order of magnitude larger than that in GaAs [22] and is comparable with what had been found for GaN [23].

[4] Index of refraction for our sample is determined by an independent experiment.

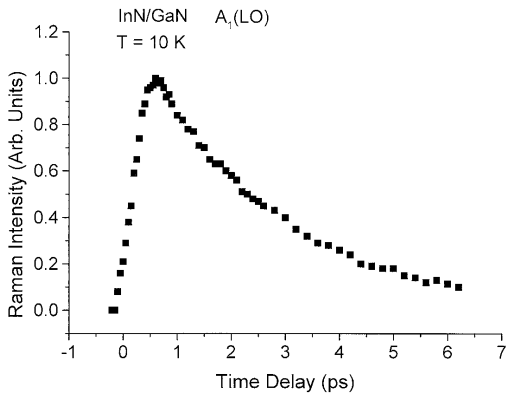

Figure 5. Integrated anti-Stokes Raman signal of A_1(LO) phonon in an InN thick film as a function of time delay, taken at $T = 10$ K.

The much larger LO–TO phonon energy splitting in wurtzite InN provides a clue to this mystery. We attribute this enormous increase of electron–LO phonon scattering rate in InN to its much larger ionicity. In general, the strength of electron–LO phonon coupling is set by the lattice–dipole interactions, which are expressed by [2]

$$\frac{1}{\gamma} = \omega_{LO}^2\left[\frac{1}{\varepsilon_\infty} - \frac{1}{\varepsilon_0}\right] = \left[\frac{\omega_{LO}^2 - \omega_{TO}^2}{\varepsilon_\infty}\right]. \quad (5)$$

This splitting is directly proportional to the lattice polarization, and is a measure of the effective charge. In GaAs, the LO–TO energy splitting is about 3 meV, while it is about 20 meV in wurtzite InN. This together with the much smaller dielectric constant of InN, lead to an expected increase of a factor of about 10 in the electron–LO phonon scattering strength, which is quite close to that observed experimentally.

Indeed, in our previous Monte Carlo simulations of electron transport in InN [24], we found that the electron–LO phonon scattering rate was quite high, rising already to approximately 1.7×10^{13} s^{-1}, for each of the two modes, at an energy of 150 meV (one $\hbar\omega_{LO}$ above the threshold for phonon emission), and assumed a value near 2.5×10^{13} s^{-1} over much of the higher energies in the nonparabolic central valley. This strong scattering process is a result of the large separation in ε_0 and ε_∞ (12.0 and 7.3, respectively), as indicated above in equation (5).

4.2. Direct measurements of the lifetimes of longitudinal optical phonon modes and their dynamics in InN [25]:

Figure 5 shows the integrated anti-Stokes Raman signal of A_1(LO) phonon in InN as a function of time delay, taken at $T = 10$ K. The excited electron–hole pair density was about $n \cong 1 \times 10^{16}$ cm^{-3}. The exponential decrease of the Raman signal found after $\Delta t = 0.6$ ps represents the decay of LO phonons. The lifetime of the A_1(LO) phonon under these experimental conditions has been determined to be $\tau = (2.5 \pm 0.2)$ ps.

In order to get better insight into the LO phonon dynamics in InN, we have repeated the same experiments as shown in figure 5 but at different lattice temperatures. The results are

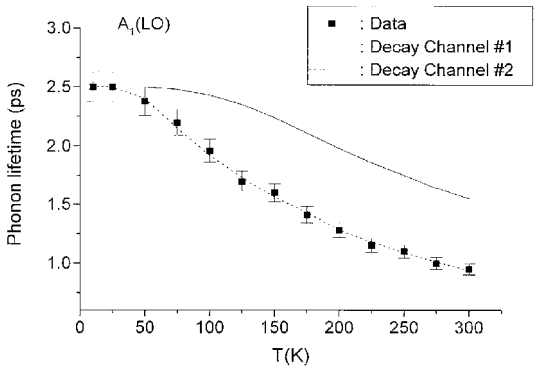

Figure 6. The temperature dependence of the population relaxation time of A_1(LO) phonon mode for an InN sample. The solid squares are experimental data. The solid and dashed curves correspond to theoretical models for the decay of the phonon. See text for discussions.

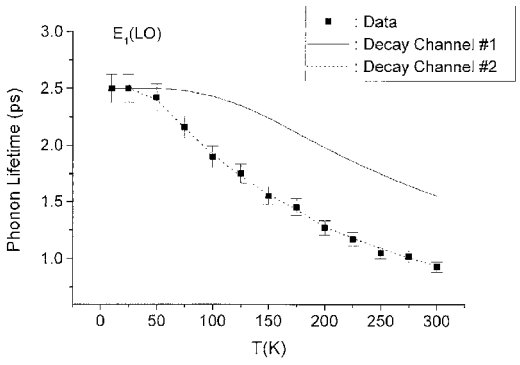

Figure 7. The temperature dependence of the population relaxation time of E_1(LO) phonon mode for an InN sample. The solid squares are experimental data. The solid and dashed curves correspond to theoretical models for the decay of the phonon. See text for discussions.

summarized in figure 6. The lifetime of A_1(LO) phonons has been found to remain almost constant at around 2.5 ps until about $T = 25$ K. As the lattice temperature increases beyond 25 K, the lifetime gradually decreases. At $T = 300$ K, it is reduced to about 1 ps. This reduction of the A_1(LO) phonon lifetime with lattice temperature is primarily due to the anharmonic decay into the lower branch phonons in InN. In general, three-phonon decay processes are the dominant decay channels in semiconductors. Klemens [26] and Ridley [27] used perturbation theory to show that the temperature-dependent part of the decay of LO phonon population $n_{\rm ph}(\omega, T)$ in semiconductors can be expressed as

$$\frac{{\rm d}n_{\rm ph}(\omega, T)}{{\rm d}t} = -n_{\rm ph}(\omega, T)[1+n_{\rm ph1}(\omega_1, T)+n_{\rm ph2}(\omega_2, T)]/\tau_0; \tag{6}$$

where τ_0 is the decay time of LO phonon at $T = 0$ K (in this case, τ_0 has been measured to be about 2.5 ps); $\omega = \omega_1 + \omega_2$; and $n_{\rm ph1}(\omega_1, T) = 1/(e^{\hbar\omega_1/k_{\rm B}T} - 1)$, $n_{\rm ph2}(\omega_2, T) = 1/(e^{\hbar\omega_2/k_{\rm B}T} - 1)$ are the occupation numbers of the lower-energy phonons into which the LO phonon modes decay. Here T is the lattice temperature and $k_{\rm B}$ is Boltzmann's constant. Equation (6) says that the temperature dependence of LO phonon lifetime is given by

$$\frac{1}{\tau(T)} = \frac{1}{\tau_0}[1 + n_{\rm ph1}(\omega_1, T) + n_{\rm ph2}(\omega_2, T)]. \tag{7}$$

There are various possible channels for the decay of zone-center A_1(LO) phonons in wurtzite InN. First of all, from our experimental data in figure 6, the decay of zone-center A_1(LO) phonons into a small wavevector LO and a small wavevector LA or TA phonons does not seem to be likely because this decay channel predicts a much larger temperature dependence of the lifetime of LO phonons than the experimental data indicate (which is not shown here). The solid curve in figure 6 represents the decay channel: $\omega_{\rm LO} \rightarrow 2\omega_{\rm LA(TA)}$ with $\hbar\omega_{\rm LA(TA)} = 299$ cm^{-1}, which is half of the energy of zone-center A_1(LO) phonons, as predicted by equation (7). We have found that, within our experimental uncertainty, the zone-center A_1(LO) phonons cannot decay into large wavevector, equal energy (but opposite momentum) LA or TA phonons, which is usually assumed in the decay of LO phonons in other III–V compound semiconductors. On the other hand, we have found that the decay channel of zone-center A_1(LO) phonons in wurtzite InN into a large wavevector TO phonon (assuming that the TO phonon dispersion curve is relatively flat across the Brillouin zone) and a large wavevector LA or TA phonon fits our experimental data very well. The dotted curve corresponds to such a decay channel: $\omega_{\rm LO} \rightarrow \omega_{\rm TO} + \omega_{\rm LA(TA)}$, as predicted by equation (7). The energies of the TO and LA or TA phonons involved in the fitting process are $\omega_{\rm TO} = 496$ cm^{-1}, $\omega_{\rm LA(TA)} = 102$ cm^{-1}, respectively. These interpretations are in good agreement with the phonon dispersion calculated by Davidov *et al* [28].

Similar experiments for the E_1(LO) phonons in InN have also been carried out. The results are shown in figure 7. The lifetime of the $E_1(LO)$ phonon has been found to be $\tau = (2.5 \pm 0.2)$ ps. Again, we have found that zone-center E_1(LO) phonons in wurtzite InN decays primarily into a large wavevector TO phonon and a large wavevector LA or TA phonon consistent with the phonon dispersion calculations in InN [28].

We note that Pomeroy *et al* [29] reported the lifetime and dynamics of the A_1(LO) phonon in InN films by analyzing the Raman line shape. The lifetime of the A_1(LO) phonon mode directly measured in our time-resolved Raman experiments is about 50% larger than what they had deduced. At this moment, it is not clear why there is a 50% difference in the measured phonon lifetimes between the time-resolved Raman scattering technique and the Raman line shape measurements.

In some narrow gap semiconductors, the decay of the optical phonons is complicated by storage of the carriers in satellite valleys, and their subsequent slow return from these valleys to the Γ valley. In InN, this is not the case, as the satellite valleys are located well above the excitation energy of the electrons in the conduction band. Thus, we achieve a very clean and direct measure of the decay of the non-equilibrium phonon distribution function.

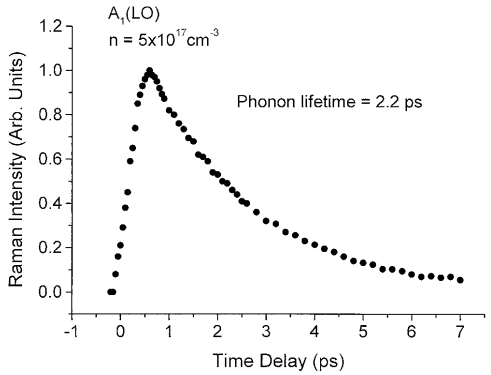

Figure 8. A typical integrated anti-Stokes Raman intensity for the $A_1(LO)$ phonon mode of an InN thick film grown on GaN, as a function of time delay, and with a photoexcited electron–hole pair density $n \cong 5 \times 10^{17}$ cm^{-3}. From the decaying part of the data the population relaxation time of the phonon can be determined.

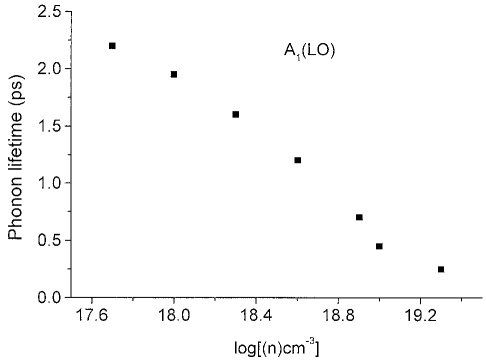

Figure 9. The measured lifetime of $A_1(LO)$ phonon mode in InN as a function of the photoexcited electron–hole pair density, ranging from 5×10^{17} to 2×10^{19} cm^{-3}.

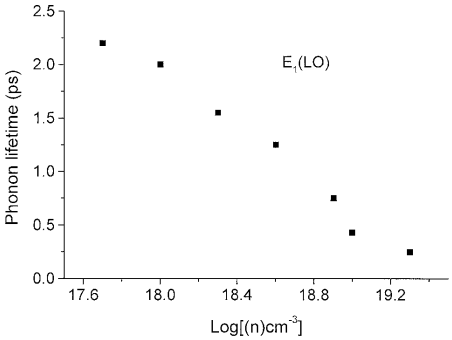

Figure 10. The measured lifetime of $E_1(LO)$ phonon mode in InN as a function of the photoexcited electron–hole pair density, ranging from 5×10^{17} to 2×10^{19} cm^{-3}.

4.3. Electron density dependence of LO phonon lifetime in InN studied by subpicosecond time-resolved Raman spectroscopy [30]

A typical integrated anti-Stokes Raman intensity for the $A_1(LO)$ phonon mode, as a function of time delay, and with a photoexcited electron–hole pair density $n \cong 5 \times 10^{17}$ cm^{-3}, is shown in figure 8. The very rapid rise of the signal from around $\Delta t = 0$ is a manifestation of an extremely large electron–LO phonon interaction in InN. It reaches a maximum at about 600 fs, indicative of the fact that at such a time delay, electrons are no longer emitting LO phonons that are detectable by our Raman spectroscopy. After about 600 fs, the anti-Stokes Raman intensity decreases with a decay constant of $\tau = (2.2 \pm 0.2)$ ps. This we define as the population relaxation time or lifetime of the $A_1(LO)$ phonon mode.

It is well known [31] that the electron plasmon couples strongly with the LO phonon mode in polar semiconductors, in particular, for a plasma density greater than 5×10^{17} cm^{-3}. We refer to the phonon-like plasmon–LO phonon-coupled mode at high electron densities as the LO phonon mode. Figure 9 shows the measured lifetime of this LO phonon mode in InN as a function of the photoexcited electron–hole pair density, ranging from 5×10^{17} to 2×10^{19} cm^{-3}. We observe that the lifetime of this LO phonon mode decreases from 2.2 ps to about 0.25 ps. We notice that similar observations for GaAs and GaN have been reported by Kash *et al* [32, 33] and Tsen *et al* [34], respectively, for which the physical interpretation remains unclear. Figure 10 shows corresponding results for the $E_1(LO)$ phonon mode. Again, a dramatic decrease of the lifetime of the $E_1(LO)$ phonons is observed, but this decrease is commensurate with that of the $A_1(LO)$ mode.

In general, the lifetime is dominated by the decay of the LO phonons into a pair of acoustic phonons, as discussed above. This is generally a relatively slow process, and cannot explain the density dependence. Moreover, screening cannot be invoked as a higher density would provide more screening and a slower response, opposite to that observed. However, Matulionis has suggested that the hot LO phonons can emit a plasmon in the relaxation process [35]. While intriguing, the mechanism for the decay via both plasmon and acoustic phonon modes has not yet been worked out. In particular, if the observed $A_1(LO)$ mode is already a coupled mode of the phonon and plasmon, it is not immediately clear how a distinct, and separate, plasmon can subsequently be emitted in the decay process. Thus, more work is needed in order to understand the mechanism by which the phonon lifetime varies with density.

5. Conclusions

In this paper, we have used subpicosecond time-resolved Raman spectroscopy to study electron–LO phonon interactions in InN. Our experimental results show that for a thick layer of InN grown on GaN the average total electron–longitudinal optical phonon scattering rate is $(5.1 \pm 1.0) \times 10^{13}$ s^{-1}. We attribute this enormous electron–LO phonon scattering rate to the extremely polar nature of InN, and the measured value is in excellent agreement with values taken from Monte Carlo simulations using the actual calculated values for these scattering rates. LO phonon dynamics in InN have also been studied by time-resolved Raman spectroscopy on a subpicosecond timescale. The lifetimes of both the $A_1(LO)$ and the $E_1(LO)$ phonons have been directly measured. From the temperature dependence of their lifetimes, we have shown that both phonons decay primarily into a large wavevector

TO phonon and a large wavevector TA or LA phonon, as the energies of these modes are consistent with the phonon dispersion relationship that have been found for wurtzite InN. Subpicosecond time-resolved Raman spectroscopy has also been used to measure the lifetime of the LO phonon modes as a function of photoexcited electron–hole pair density ranging from 5×10^{17} to 2×10^{19} cm^{-3} in InN. The lifetime has been found to decrease from 2.2 to 0.25 ps for both the A_1(LO) and E_1(LO) phonon modes. Previous measurements on LO phonon lifetimes in GaAs and GaN have also shown such a density dependence, and the present experimental findings demonstrate that carrier density dependence of the LO phonon lifetime is likely a universal phenomenon in polar semiconductors. The cause of such density dependence is not currently understood, and more work is needed.

Acknowledgments

This work was supported by the National Science Foundation. We would like to acknowledge W J Schaff for providing InN sample.

References

[1] Pankove J I and Moustakas T D 1997 *Gallium Nitride* (*Semiconductors and Semimetals* vol 50) ed R K Willardson and E R Weber (New York: Academic)
[2] For a review, see Bhuiyan A G, Hashimoto A and Yamamoto A 2003 *J. Appl. Phys.* **94** 2779
[3] Mohammad S N and Morkoc H 1996 *Prog. Quantum Electron.* **20** 361
[4] O'Leary S K, Foutz B E, Shur M S, Bhapkar U V and Eastman L F 1998 *J. Appl. Phys.* **83** 826
[5] Bellotti E, Doshi B K, Brennan K F, Albrecht J D and Ruden P P 1999 *J. Appl. Phys.* **85** 916
[6] Foutz B E, O'Leary S K, Shur M S and Eastman L F 1999 *J. Appl. Phys.* **85** 7727
[7] Conwell E M 1967 *High Field Transport in Semiconductors* (New York: Academic)
[8] Hamaguchi C and Inoue M 1992 *Proc. 7th Int. Conf. on Hot Carriers in Semiconductors* (New York: Hilger)
[9] Lu H, Schaff W J, Eastman L F, Wu J, Walukiewicz W, Look D C and Molnar R J 2003 *Proc. Mat. Res. Soc. Symp.* vol 743, p L4.10
[10] Tsen K T 2001 *Ultrafast Phenomena in Semiconductors* ed K T Tsen (New York: Springer) pp 191–259
[11] Tsen K T 2001 *Ultrafast Physical Processes in Semiconductors* (*Semiconductors and Semimetals* vol 67) ed K T Tsen (Boston, MA: Academic) pp 109–49
[12] Tsen K T 2004 *Ultrafast Dynamical Processes in Semiconductors* (*Springer Topics in Applied Physics* vol 92) ed K T Tsen (Heidelberg: Springer) pp 193–258
[13] Tsen K T 2005 *Non-Equilibrium Dynamics of Semiconductors and Nanostructures* ed K T Tsen (New York: CRC Press) pp 179–213
[14] Tsen K T, Kiang J G, Ferry D K, Lu H, Schaff W J, Lin H-W and Gwo S 2007 *Appl. Phys. Lett.* **90** 172108
[15] Carrier P and Wei S-H 2005 *J. Appl. Phys.* **97** 033707
[16] Inushima T, Mamutin V V, Vekshin V A, Ivanov S V, Sakon T, Motokawa M and Ohoya S 2001 *J. Cryst. Growth* **227/228** 481
[17] Davydov V Yu, Klochikhin A A, Seisyan R P, Emtsev V V, Ivanov S V, Bechstedt F, Furthmüller J, Harima H, Mudryi A V, Aderhold J, Semchinova O and Graul J 2002 *Phys. Status Solidi* b **229** R1
Davydov V Yu, Klochikhin A A, Emtsev V V, Ivanov S V, Vekshin V V, Bechstedt F, Furthmüller J, Harima H, Mudryi A V, Hashimoto A, Yamamoto A, Aderhold J, Graul J and Haller E E 2002 *Phys. Status Solidi* b **230** R4
Davydov V Yu, Klochikhin A A, Emtsev V V, Kurdyukov D A, Ivanov S V, Vekshin V A, Bechstedt F, Furthmüller J, Aderhold J, Graul J, Mudryi A V, Harima H, Hashimoto A, Yamamoto A and Haller E E 2002 *Phys. Status Solidi* b **234** 787
[18] Wu J, Walukiewicz W, Yu K M, Ager J W III, Haller E E, Lu H, Schaff W J, Saito Y and Nanishi Y 2002 *Appl. Phys. Lett.* **80** 3967
[19] Wu J, Walukiewicz W, Yu K M, Ager J W III, Haller E E, Lu H and Schaff W J 2002 *Appl. Phys. Lett.* **80** 4741
[20] Yamamoto A, Sugita K, Takatsuka H, Hashimoto A and Davydov V Yu 2004 *J. Cryst. Growth* **261** 275
[21] Xu Y N and Ching W Y 1993 *Phys. Rev.* B **48** 4335
[22] Kash J A, Tsang J C and Hvam J M 1985 *Phys. Rev. Lett.* **54** 2151
[23] Tsen K T, Ferry D K, Botchkarev A, Sverdlov B, Salvador A and Morkoc H 1997 *Appl. Phys. Lett.* **71** 1852
[24] Liang W, Tsen K T, Ferry D K, Lu H and Schaff W J 2004 *Appl. Phys. Lett.* **84** 3681
[25] Tsen K T, Kiang J G, Ferry D K, Lu H, Schaff W J, Lin H-W and Gwo S 2007 *Appl. Phys. Lett.* **90** 152107
[26] Klemens P G 1966 *Phys. Rev.* **148** 845
[27] Ridley B K 1996 *J. Phys.: Condens. Matter* **8** L511
[28] Davydov V Yu, Emtsev V V, Goncharuk I N, Smirnov A N, Petrikov V D, Mamutin V V, Vekshin V A, Ivanov S V, Smirnov M B and Inushima T 1999 *Appl. Phys. Lett.* **75** 3297
[29] Pomeroy J W, Kuball M, Lu H, Schaff W J, Wang X and Yoshikawa A 2005 *Appl. Phys. Lett.* **86** 223501
[30] Tsen K T, Kiang J G, Ferry D K, Lu H, Schaff W J, Lin H-W and Gwo S 2007 *J. Phys.: Condens. Matter* **19** 236219
[31] Abstreiter G, Cardona M and Pinczuk A 1986 *Light Scattering in Solids IV* ed M Cardona and G Güntherodt (New York: Springer) p 5
[32] Kash J A and Tsang J C 1988 *Solid State Electron.* **31** 419
[33] Tsang J C, Kash J A and Jha S S 1985 *Physica* B **134** 184
[34] Tsen K T, Kiang Juliann G, Ferry D K and Morkoc H 2006 *Appl. Phys. Lett.* **89** 262101
[35] Matulionis A, private communications